Metal-insulator phase transition in a VO_2 thin film observed with terahertz spectroscopy

Peter Uhd Jepsen
COM•DTU, Technical University of Denmark, DK-2800 Kgs. Lyngby, Denmark

Bernd M. Fischer, Andreas Thoman, and Hanspeter Helm
Freiburg Materials Research Center, University of Freiburg, Stefan-Meier-Strasse 21, D-79104 Freiburg, Germany

J. Y. Suh, René Lopez,* and R. F. Haglund, Jr.
Department of Physics and Astronomy, Vanderbilt University, Nashville, Tennessee 37235, USA
(Received 2 March 2006; revised manuscript received 9 August 2006; published 6 November 2006)

We investigate the dielectric properties of a thin VO_2 film in the terahertz frequency range in the vicinity of the semiconductor-metal phase transition. Phase-sensitive broadband spectroscopy in the frequency region below the phonon bands of VO_2 gives insight into the conductive properties of the film during the phase transition. We compare our experimental data with models proposed for the evolution of the phase transition. The experimental data show that the phase transition occurs via the gradual growth of metallic domains in the film, and that the dielectric properties of the film in the vicinity of the transition temperature must be described by effective-medium theory. The simultaneous measurement of both transmission and phase shift allows us to show that Maxwell-Garnett effective-medium theory, coupled with the Drude conductivity model, can account for the observed behavior, whereas the widely used Bruggeman effective-medium theory is not consistent with our findings. Our results show that even at temperatures significantly above the transition temperature the formation of a uniform metallic phase is not complete.

DOI: 10.1103/PhysRevB.74.205103 PACS number(s): 71.30.+h, 42.25.Dd, 42.70.Gi, 07.57.Pt

I. INTRODUCTION

Bulk vanadium dioxide (VO_2) undergoes a phase transition from semiconductor to metal at a temperature near 68 °C.[1] Associated with the phase transition are a change of conductivity by several orders of magnitude, strong changes of the optical properties at all wavelengths, and a structural transition from the low-temperature monoclinic phase to a tetragonal metallic phase. There is a marked hysteresis associated with both the electrical and the optical properties of VO_2, indicating that the phase transition is of first order. The evolution of the phase transition depends strongly on the morphology of the material. The transition temperature as well as the width of the hysteresis can be strongly modified by nanostructuring of the VO_2 material[2] and by interface effects in epitaxially grown thin films.[3] Here we discuss the properties of thin films of polycrystalline VO_2.

The phase transition in a thin semiconducting film of VO_2 is initiated at seed points in the film, and the metallic domains then grow and spread as the temperature is increased towards and beyond the transition temperature. Hence in the vicinity of the transition temperature the semiconducting and the metallic domains coexist. This spatial inhomogeneity of the thin film strongly influences the effective dielectric properties of the film. Hood *et al.* used effective-medium theory (EMT) to interpret transmission measurements at 38.5 GHz,[3] and Choi *et al.* found that effective-medium theory must be applied to interpret midinfrared spectroscopic measurements.[4] There have been several observations of percolation behavior of VO_2 films, i.e., the formation of a macroscopic conductive path through the sample. Recently Rozen *et al.* applied EMT to interpret conductivity measurements of nanostructured VO_2 films.[5] Common to these reports is that the Bruggeman EMT (Ref. 6) was used since this particular EMT describes percolation. However, the Maxwell-Garnett EMT (Ref. 7) offers an alternative description of the dielectric properties of a composite material. There are several comparative studies of the two EMT's, and even though the Maxwell-Garnett theory does not account for percolation, and is derived under the assumption of a low volume fraction of the conductive domains, there are reports favoring this EMT over the Bruggeman EMT.[8,9]

In this work we perform terahertz time-domain spectroscopy (THz-TDS) in the frequency range 0.1–1.5 THz. With this technique we can measure the transmission amplitude and phase of a broadband THz signal transmitted through a thin film of VO_2 deposited on a dielectric substrate. The THz range is useful in studies of conductive systems since it is a contact-free measurement which probes the high-frequency conductivity of the system, in contrast to the static conductivity measured with standard four-point probes. Hence we expect to be independent of the formation of macroscopic conductivity paths through the sample. The THz frequency range falls below the optical phonon resonances of VO_2, and hence it is possible to measure the dielectric response that arises solely from the conductivity of the sample.

It turns out that the simultaneous measurement of both transmission amplitude and phase shift over a broad spectral range allows a comparison of different effective-medium theories as well as different conductivity models. In contrast to THz transmission measurements on homogeneous thin films[10] we observe a phase delay when the THz signal is transmitted through the VO_2 film above the transition temperature. The spectral shape, combined with the temperature dependence of both transmission amplitude and phase shift, shows that the Maxwell-Garnett EMT coupled with the classical Drude model for the description of the conductivity of the metallic domains is best suited to describe the THz optical properties of the VO_2 film in the vicinity of the transition temperature.

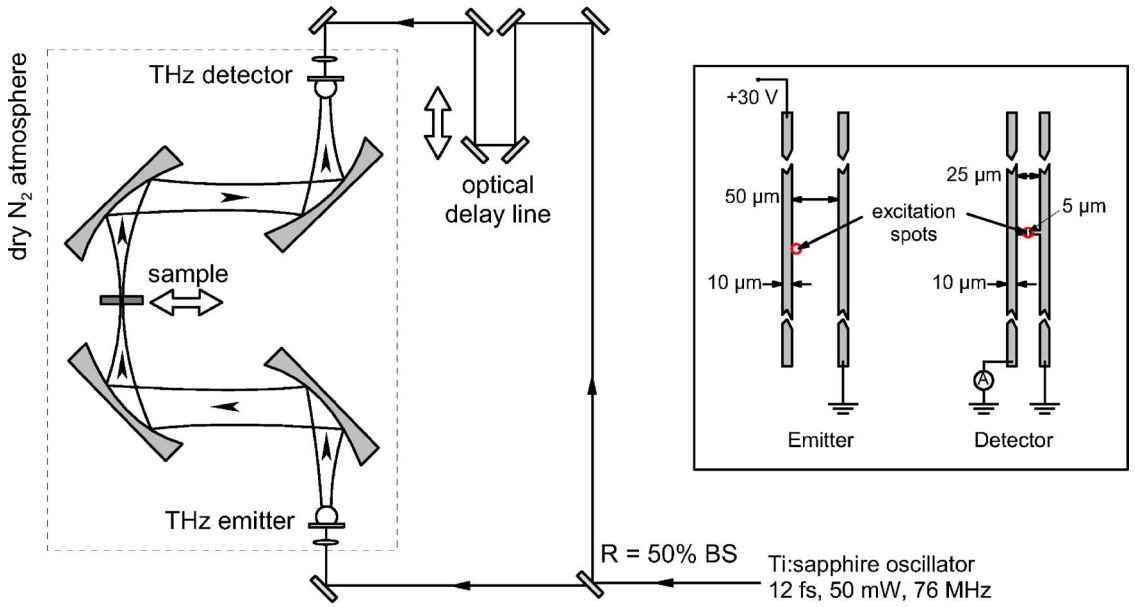

FIG. 1. (Color online) Experimental setup for terahertz time-domain spectroscopy (THz-TDS).

The paper is structured as follows. In the following we describe the sample fabrication in Sec. II A and experimental techniques in Sec. II B. Then we present the methods used in the spectroscopic analysis of the experimental data in Sec. III A, and summarize the two effective-medium theories used in the interpretation of the results in Sec. III B. The experimental results are then presented and discussed in Sec. IV and Sec. V. Finally the conclusions of the paper are summarized in Sec. VI.

II. EXPERIMENTAL METHODS

A. Sample fabrication

A VO_2 film of 160 nm thickness was grown on a glass substrate of 150 μm thickness. A vanadium metal target was ablated in an oxygen ambient (5 mTorr) by a KrF excimer laser at a wavelength of 248 nm and a fluence of 4 J/cm^2. Approximately 10^5 laser pulses were required to deposit the film. The target-substrate distance was typically 7 cm. The as-deposited film is amorphous and exhibits an incomplete stoichiometry close to $VO_{1.7}$ as determined by Rutherford backscattering (RBS). After conversion to VO_2 by thermal oxidation at 200 mTorr of O_2 and a temperature of 450 °C, the phase and crystallinity were confirmed by x-ray diffraction (XRD) while stoichiometry was verified by RBS. In some cases, x-ray powder diffraction analysis on samples grown under these conditions showed traces of V_2O_5. However, the RBS measurements showed that over areas of several square millimeters, comparable with the THz spot size used for spectroscopy, the film composition is uniformly VO_2.

B. THz time-domain spectroscopy

In order to measure the complex dielectric properties of the VO_2 thin film we use the Freiburg THz time-domain spectroscopy (THz-TDS) system.[11,12] THz-TDS relies on the generation and detection of ultrashort, broadband electromagnetic transients with frequency components spanning over the lowest region of the far infrared, typically covering the frequency region 0.1–3 THz, or 3–100 cm^{-1}. The experimental setup is illustrated in Fig. 1.

A beam of femtosecond laser pulses is split in two sections. One section is used to generate the THz transient by excitation of a biased, photoconductive antenna, while the other section acts as a gate in the photoconductive detector. The temporal shape of the THz transient is recorded by gradually changing the relative delay between the THz transient and the gate pulse while monitoring the current induced in the external circuitry by the THz field.

As illustrated in Fig. 2 the THz beam is collimated and focused through the sample mount, and transmitted through either a reference aperture or a sample aperture. The reference aperture is covered by a section of the sample consist-

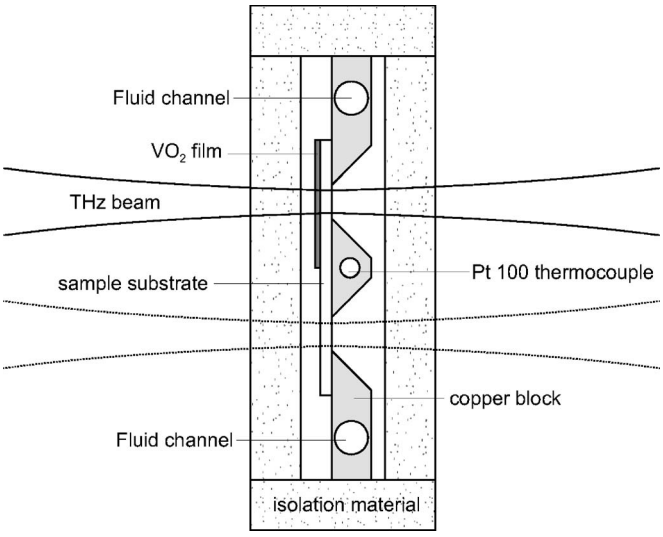

FIG. 2. Detailed view of the thermally isolated sample mount.

ing of the substrate alone, and the sample aperture is covered by a section of the sample consisting of substrate and VO_2 film. The configuration of the off-axis paraboloidal mirrors ensures a frequency-independent spot size of the THz beam on the sample.

In this manner we determine the transmission amplitude and transmission phase in the frequency region 0.1–2 THz, the higher-frequency limit being determined by increasing attenuation of the THz signal at high frequencies in the substrate material.

The temperature of the sample was controlled by circulating oil from an oil bath, and determined by a Pt-100 thermocouple mounted between the two apertures of the copper sample mount. The sample was in good thermal contact with the mount, and the entire mount was isolated from the surroundings with a thick layer of styrofoam. During each measurement the sample temperature was constant to within ±0.1 K. We estimate that the absolute temperature was accurate to within ±0.5 K except for the transmission measurements with 800 nm light, where apertures in the isolation materials had to be drilled in front of the samples in order to transmit the optical beam. This led to a slightly lower temperature of the sample than measured in the copper block. We estimate this systematic temperature drop to be less than 2 K.

III. NUMERICAL AND THEORETICAL BACKGROUND

A. Spectroscopic analysis

THz-TDS measures the complex transmission function $A\exp(i\phi)$ of the sample within the bandwidth of the THz signal. This transmission function is linked to the dielectric function of the thin film of thickness d and with a complex index of refraction $\hat{n}_2=n_2+i\kappa_2$. The index of refraction of the substrate is $\hat{n}_3=n_3+i\kappa_3$, and its thickness is L. The extinction coefficient is related to the absorption coefficient through $\kappa=\alpha c/2\omega$. The substrate used in our experiments displayed considerable absorption which needs to be taken into account in the analysis in order to obtain quantitative results from the measurements.

We use the standard theory of electromagnetic plane wave propagation through a stratified medium.[13] Each layer in the structure is modeled by a characteristic complex-valued 2×2 matrix,

$$\underline{\underline{M}} = \begin{bmatrix} \cos \hat{k}l & -\frac{i}{\hat{n}} \sin \hat{k}l \\ -i\hat{n} \sin \hat{k}l & \cos \hat{k}l \end{bmatrix}, \tag{1}$$

where $\hat{n}=n+i\kappa$ is the complex index of refraction of the layer, $\hat{k}=\hat{n}\omega/c$ is the complex wave number. Propagation through a multilayered system can then be calculated by multiplication of the characteristic matrices for each layer. For a layered sample surrounded by air the transmission coefficient is then

$$t = \frac{2}{M_{11}+M_{21}+M_{12}+M_{22}}, \tag{2}$$

where M_{ij} are the elements of the transfer matrix. In our experiments the VO_2 film was deposited on a substrate of 150 μm thickness, so the standard procedure of truncating the time-domain data before the appearance of echoes in the time domain cannot be applied. Hence we need to model the full sample structure in order to compare the experimental results with models of the dielectric function of the thin film.

The experiment measures the amplitude A and phase ϕ of the ratio

$$\frac{E_{\text{sam}}(\omega)}{E_{\text{ref}}(\omega)} \equiv A\exp(i\phi) = \frac{M_{11}^{\text{ref}}+M_{21}^{\text{ref}}+M_{12}^{\text{ref}}+M_{22}^{\text{ref}}}{M_{11}^{\text{sam}}+M_{21}^{\text{sam}}+M_{12}^{\text{sam}}+M_{22}^{\text{sam}}}, \tag{3}$$

where the reference and sample matrix are given by

$$\underline{\underline{M}}_{\text{ref}} = \underline{\underline{M}}_{\text{air}} \cdot \underline{\underline{M}}_{\text{substrate}}, \tag{4}$$

$$\underline{\underline{M}}_{\text{sam}} = \underline{\underline{M}}_{\text{film}} \cdot \underline{\underline{M}}_{\text{substrate}}. \tag{5}$$

The complex index of refraction of the thin film can hence, at least in principle, be obtained by solving Eq. (3) with respect to n_2 and κ_2. A substrate with a thickness comparable to the wavelength of the THz light will result in strong etalon artifacts in the transmission function. If the index of refraction n_3 and the extinction coefficient κ_3 of the substrate is known then the fringes in the transmission spectrum caused by the etalon effect can be removed by the operation outlined here. However, in practice these quantities are often not known with sufficiently high precision, so some contamination of the dielectric spectrum of the thin film due to multiple reflections in the substrate material must be expected, and is indeed observed in our experimental data. We have therefore chosen to compare the measured transmission amplitude and phase shift with model predictions of these quantities instead of actually inverting Eq. (3).

B. Effective-medium theories and the Drude model

As discussed in the Introduction there is substantial evidence that the phase transition in VO_2 films occurs by growth of conductive domains, and our experimental data can only be explained within this picture. If the thin film is inhomogeneous in its spatial structure then the connection between the local microscopic dielectric function and the macroscopic effective dielectric function must be established. This connection is described by different variations of effective-medium theory, with the Bruggeman[6] and the Maxwell-Garnett[7] EMT's as the most widely used descriptions of the effective dielectric function. Both models relate the effective, macroscopic dielectric function ϵ_{eff} of a sample, consisting of two different domains, to the dielectric functions of each of these domains. The domains are assumed to be of dimensions much smaller than the wavelength of the radiation but large enough to be described by a dielectric function. At THz frequencies these criteria are easily met. The relation between the effective dielectric function

ϵ and the dielectric functions of the insulating and metallic regions, ϵ_i and ϵ_m, respectively, are in the Bruggeman EMT and the Maxwell-Garnett EMT described as

$$\epsilon_{\text{eff}}^{\text{BR}} = \tfrac{1}{4}\{\epsilon_i(2-3f) + \epsilon_m(3f-1) + \sqrt{[\epsilon_i(2-3f) + \epsilon_m(3f-1)]^2 + 8\epsilon_i\epsilon_m}\}, \quad (6)$$

$$\epsilon_{\text{eff}}^{\text{MG}} = \epsilon_i \frac{\epsilon_m(1+2f) - \epsilon_i(2f-2)}{\epsilon_i(2+f) + \epsilon_m(1-f)}, \quad (7)$$

where f is the volume fraction of conductive regions. Here we use the expressions valid for metallic inclusions of spherical shape. The two EMT's discussed here are conceptually quite different, and the validity regimes of the two theories are still subject to discussion and investigations. In general terms, the Maxwell-Garnett EMT is expected to be valid at low volume fractions f since it is assumed that the conductive domains are spatially separated. In contrast, the Bruggeman EMT makes no assumptions about the volume fraction. Many factors, such as the size and shape of the conductive domains, influence the predictions of both models. The Bruggeman EMT has been applied for the description of various properties of the semiconductor-metal transition in VO_2.[3–5] This particular EMT has been favored because it predicts percolation behavior when the volume fraction of the conductive domains is large enough to form a continuous conducting path throughout the sample. We find that the Maxwell-Garnett EMT is superior to the Bruggeman EMT in explaining the THz-frequency dielectric function of the VO_2 film near the transition temperature.

The dielectric function of the metallic domains of the VO_2 film can be modeled by the classical Drude model, possibly with the generalization suggested by Smith[14] to include memory effects such as preferred backscattering and localization of charges in poor conductors,

$$\epsilon_m(\omega) = \epsilon_\infty - \frac{\omega_p^2}{\omega(\omega + i\Gamma)}\left(1 + \frac{ic\Gamma}{\omega + i\Gamma}\right), \quad (8)$$

where ω_p is the plasma frequency ($\omega_p^2 = Ne^2/\epsilon_0 m^*$), $\omega = 2\pi\nu$ is the cyclic frequency, and Γ is the scattering rate, related to the mobility μ of the charge carriers through $\Gamma = e/m^*\mu$. The parameter c represents the fraction of the original velocity of the electron that is retained after a scattering event. Negative values of c correspond to preferred backscattering. The generalized Drude conduction model with inclusion of backscattering has been applied by Turner *et al.* in the description of conductivity in strongly localized systems such as TiO_2 nanoparticles.[15] Recently similar experimental results in TiO_2 were interpreted by Hendry *et al.* using effective-medium theory and the Drude model without the additional backscattering term.[9]

We will assume that the plasma frequency and the scattering rate remain constant in the temperature range in this study (20 °C–100 °C) and within the frequency range considered here (0.1–1.5 THz). We assume that the dielectric function of the insulating regions of the VO_2 film equals the high-frequency dielectric function of the metallic domains, $\epsilon_i = \epsilon_\infty$. This is the limiting value of the Drude dielectric function for low free-carrier concentration.

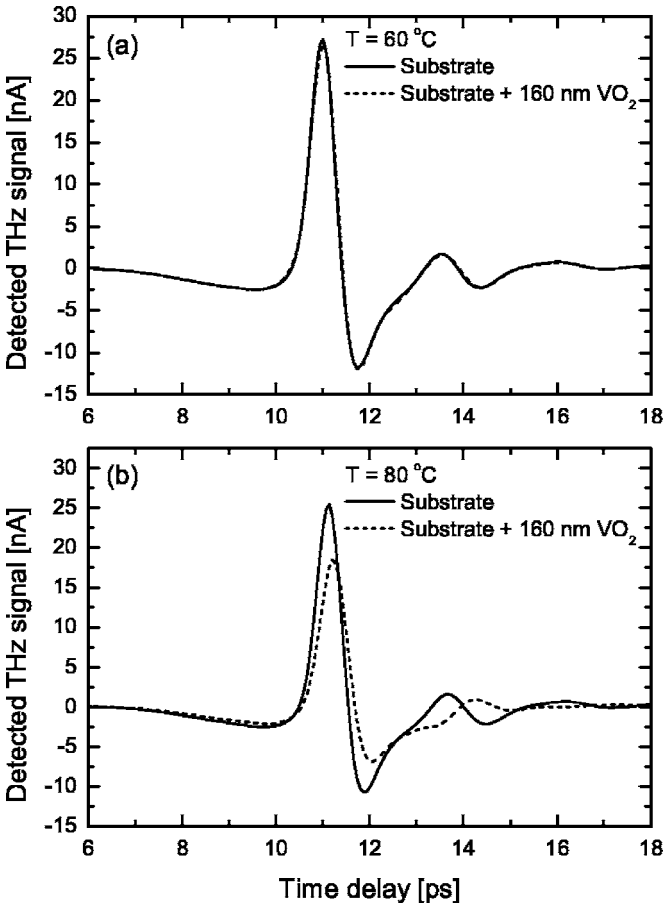

FIG. 3. THz signals transmitted through the bare substrate compared to the transmitted signal through the substrate and VO_2 film at a temperature of (a) 60 °C and (b) 80 °C. Notice the slight delay of the THz signal through the metallic VO_2 film at high temperatures.

IV. RESULTS

We measured the complex transmission through a 160 nm thick VO_2 film deposited on a 150 μm thick glass substrate. The glass substrate was independently characterized. Significant absorption as well as some dispersion was observed in the frequency range 0.1–2 THz. Both are taken into account in the following analysis.

We determined the optical properties of the thin VO_2 film in the temperature range from 25 °C–100 °C. In Fig. 3 the THz signals transmitted through the thin film on the substrate are compared to the THz signals transmitted through the substrate alone.

The transmission at $T = 60$ °C, below the transition temperature, is shown in part (a) of the figure, and the transmission at $T = 80$ °C, well above the transition temperature, is shown in part (b) of the figure. The THz beam path was purged with dry nitrogen in order to avoid absorption by water vapor.[16] The complicated shape of the signal following

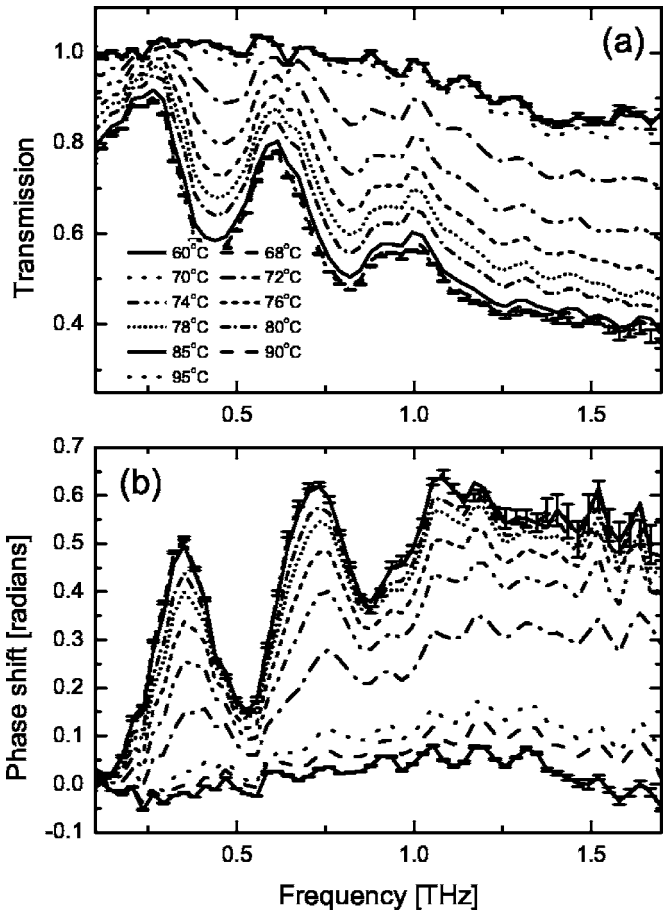

FIG. 4. Temperature dependence of the (a) amplitude ratio and (b) phase difference of the complex transmission through the VO_2 film and the substrate with respect to transmission through the bare substrate. The strong oscillations at low frequencies are due to multiple reflections in the sample substrate, as explained in the text.

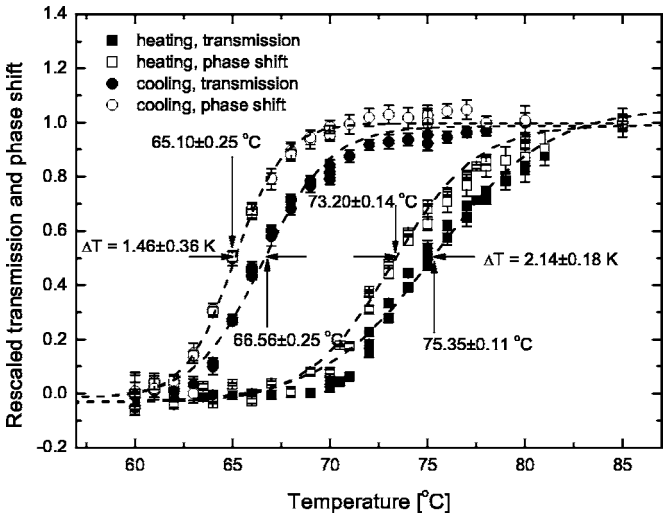

FIG. 5. Normalized and rescaled THz transmission and phase shift curves across the metal-insulator transition in the VO_2 film during several heating and cooling cycles. The curves shown as dashed lines are sigmoidal fits to the experimental data. The temperatures indicate the turning point of these sigmoidal fits.

the main part of the pulse is due to multiple reflections in the substrate. At low temperatures the THz signal is transmitted through the VO_2 film with very little disturbance. As the temperature is increased and the film switches toward its metallic state we observe significant modifications to the THz signal. First, the amplitude decreases due to increased absorption and reflection losses. Second, we observe a delay of the pulse which is not present below the transition temperature.

The observed *delay* of the transmitted THz signal is a direct indicator of domain growth as the mechanism behind the metal-insulator phase transition. We have earlier observed a phase *advance* of a THz pulse transmitted through a thin photoexcited surface layer of a semiconductor with a homogeneous distribution of free carriers, compared to an unexcited surface. This phase advance is a result of the complex transmission coefficients in and out of the conductive layer, and therefore a quite fundamental property of a thin conductive layer.[10] Hence the phase delay observed here cannot be explained if the conductive film is assumed to be homogeneous, whereas effective-medium theory reproduces the sign of the phase shift, as will be shown below.

In Fig. 4 the frequency-dependent transmission amplitude and phase shift through the VO_2 film and the substrate relative to transmission through the bare substrate is shown. Below the expected transition temperature the transmission amplitude is close to unity, and the phase shift is close to zero. Each set of data is the frequency-domain average of 5–10 data sets recorded at each temperature. The error bars indicate the standard deviation of the mean transmission amplitude and phase shift. The drop in transmission at frequencies above 1 THz below the transition temperature is probably an experimental artifact due to slight differences in the beam path through the sample and reference apertures. As the temperature of the sample approaches and crosses the transition temperature the frequency-dependent transmission decreases, and the phase shift increases. The strong oscillations in both the amplitude and the phase spectra are due to multiple reflections of the THz signal in the substrate. At high temperatures the reflectivity of the VO_2 film increases, and consequently the modulation depth of the interference fringes increases.

The spectral shape of both transmission amplitude and phase remains constant at all temperatures. In Fig. 5 we therefore show the average transmission and phase shift, in the frequency range 0.3–1.2 THz. In order to compare the temperature behavior of transmission amplitude and phase shift, we have rescaled and normalized the data sets so that their values approach zero at low temperatures and unity at high temperatures. The experimental data points in Fig. 5 were obtained from four individual heating and cooling cycles. The temperature behavior shown here and in Fig. 4 was recorded during several hours due to the relatively long acquisition time required for a reasonable quality of the THz data.

The solid and open squares represent the temperature dependence of the transmission amplitude and phase shift, respectively, during the heating part of the temperature cycle. The solid and open circles represent the temperature dependence of the transmission amplitude and phase shift, respectively, during cooling part of the temperature cycle. The

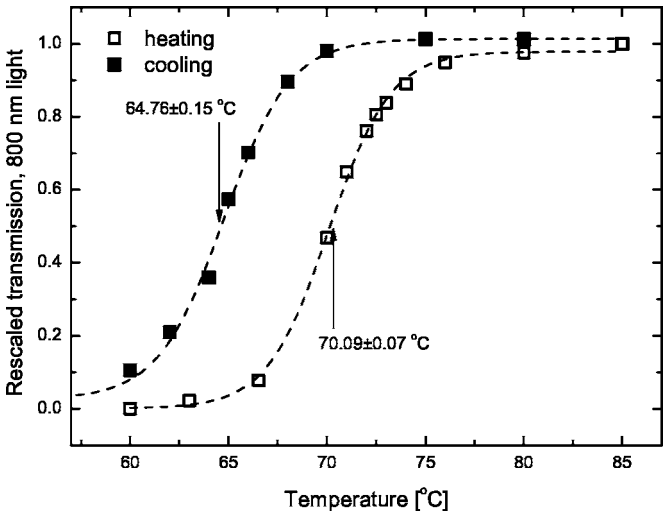

FIG. 6. Normalized and rescaled transmission of 800 nm light through the VO_2 film during a heating and cooling cycle.

dashed curves shown together with the experimental data are sigmoidal fits to the experimental transmission amplitudes and phase shifts, and are meant only as guides to the eye. We observe a significant hysteresis of the switching behavior, with an 8–9 K difference between the 50-percent point of the heating curves and the cooling curves. This typical hysteresis behavior is also observed in all other reported frequency ranges. The interesting information contained in the figure is that there is a clear difference in the switching temperature of the transmission amplitude and the phase shift. Both during heating and during cooling the transmission amplitude switches at a significantly higher temperature than the phase shift. Furthermore, the transition temperature during heating is significantly higher (73 °C for the phase shift and 75 °C for the transmission amplitude) than the expected transition temperature of 68 °C observed both in dc conductivity measurements and optical transmission measurements on bulk or thin-film VO_2 samples.

In Fig. 6 we show the transmission of an 800 nm laser beam through the same sample as a function of temperature during a full heating and cooling cycle. For this measurement we drilled small holes in the styrofoam isolation material of the sample chamber to allow passage of the near-IR beam. The spot size of the 800 nm beam on the sample was approximately 2 mm, comparable to the spot size of the THz beam. The transition temperature for the 800 nm light is now near 70 °C during heating and near 65 °C during cooling. The slightly high transition temperature compared to the expected 68 °C for bulk and thin-film VO_2 is probably due to the small openings in the styrofoam isolation leading to a small temperature drop of the sample with respect to the point in the copper block where the temperature was measured.

In summary, we need to explain the following main features of the experimental results: (1) The higher transition temperature in the THz range compared to measurements at visible and near-IR wavelengths, (2) the significant difference in switching temperature of the THz transmission amplitude and THz phase shift, (3) the magnitude of the THz transmission amplitude and THz phase shift, (4) and the sign of the THz phase shift.

V. DISCUSSION

The scenario where the thin film consists of a homogeneous, conducting material with temperature-dependent carrier concentration, is inconsistent with the sign and magnitude of the observed phase shift as well as the increased transition temperature. If instead we model the phase transition by growth of conductive domains in the plane of the thin film and use effective-medium theory to calculate the macroscopic dielectric function of the film all the experimental observations are verified in a quantitative manner, as will be shown below.

We can use our experimental data to test the validity of the Bruggeman EMT and the Maxwell-Garnett EMT. In Fig. 7 the transmission amplitude and phase shift, as calculated on the basis of Maxwell-Garnett EMT and Bruggeman EMT, are shown. Both transmission amplitude and phase shift are calculated relative to transmission through the bare substrate. The transmission amplitude and phase shift are shown in the temperature range 50 °C–100 °C, and in the frequency range 0.1–2 THz.

We used a free-carrier concentration in the metallic domains of $n=1.3\times10^{22}$ cm^{-3}, an effective mass of the charge carriers $m^*=2m_e$, where m_e is the free electron mass, and a mobility of $\mu=2$ cm^2/V s. The values of these fundamental parameters are selected according to estimates.[4] However, the behavior of the optical properties in the THz range is quite insensitive to the exact values of these parameters. Because of the expected high scattering rate we tried to incorporate memory effects in the Drude model as discussed in the preceding section, but this made agreement between the model and our experimental results very poor. The reason is that the magnitude of the dielectric function at frequencies below the plasma frequency is decreased significantly by the inclusion of backscattering in the conduction model. This is a consequence of the reduced dc conductivity and the transfer of oscillator strength from dc to high frequencies in such a system.

We modeled the temperature dependence of the volume fraction of the metallic domains with a Boltzmann function,

$$f(T) = f_{\max}\left(1 - \frac{1}{1+\exp[(T-T_0)/\Delta T]}\right), \tag{9}$$

with a switching point $T_0=68$ °C and a width of the transition $\Delta T=2$ °C. $f_{\max}$ is the volume fraction of the metallic domain at the highest temperature investigated in the experiment. We used $f_{\max}=0.95$ for the results shown in Fig. 7.

In the limit $f=1$ both the Maxwell-Garnett and the Bruggeman effective dielectric function approaches that of the conductive phase of the mixture. Hence as the volume fraction of the metallic phase approaches unity both theories predict a reversal of the sign of the phase shift. Even at the highest temperature of 100 °C we see no experimental indication of the onset of this sign reversal of the phase change. This leads us to the interesting conclusion that the phase transition apparently remains incomplete even at temperatures significantly above the transition point. There are at least two possible explanations for this observation: (1) The phase transition really is incomplete; or (2) there is a small

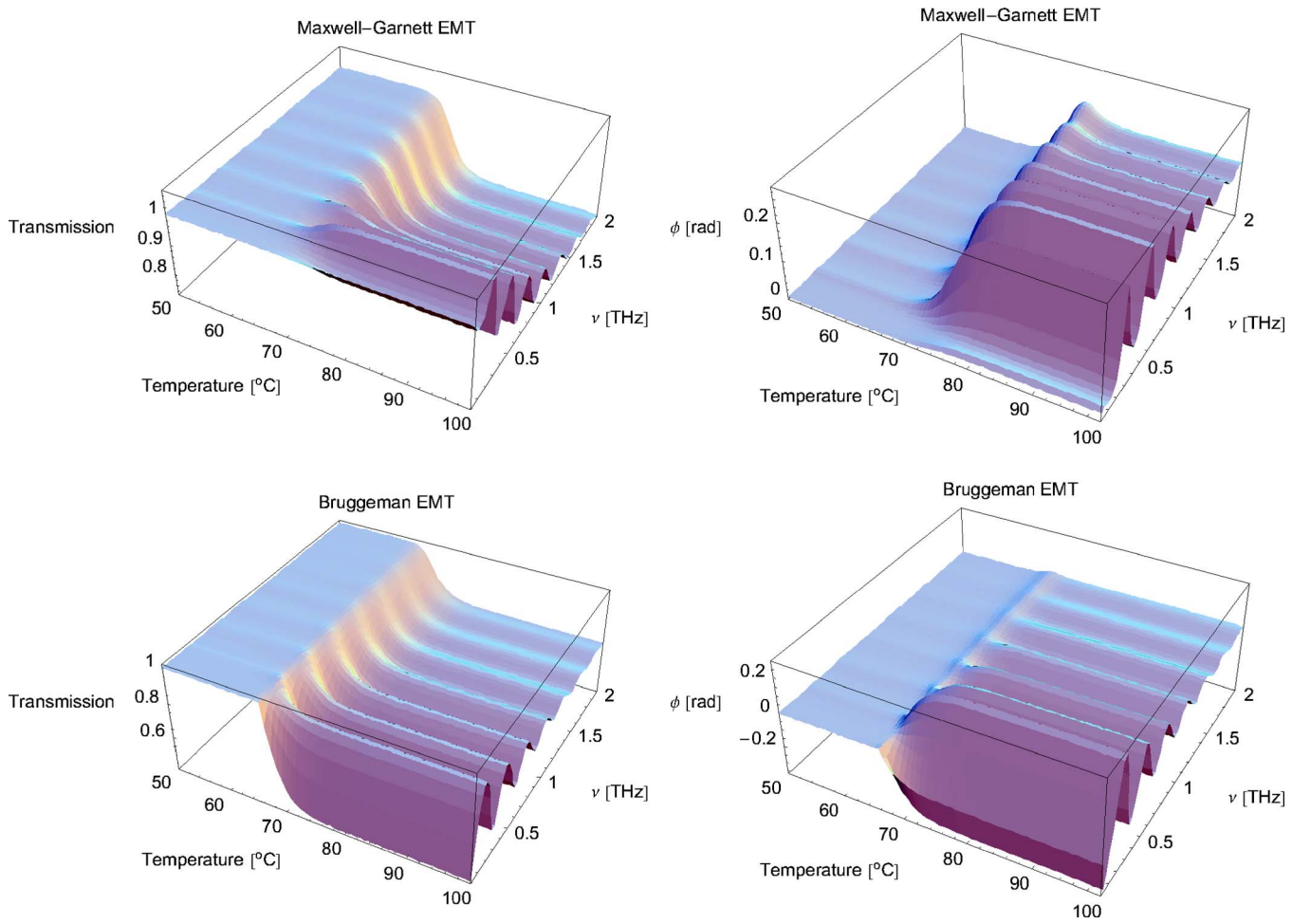

FIG. 7. (Color online) Transmission amplitude and phase shift as calculated with Maxwell-Garnett EMT and Bruggeman EMT.

void fraction in the film for which the model does not account. Explanation (1) is contradicted by recent measurements of the optical response of VO_2 in which the phase transition is induced by a femtosecond laser pulse. These measurements show that the surface plasmon resonance, indicating the formation of the metallic state, is fully formed in less than 200 fs after the transition is initiated by an ultrafast laser pulse, and that the shape and amplitude of the spectrum are identical to what is observed in an adiabatic thermally induced transition.[17,18] On the other hand, explanation (2) is bolstered by the fact that the structure of even 100 nm thick VO_2 films shows significant granularity,[19] quite possibly indicating either a modest void fraction or regions of nonstoichiometric vanadium oxides that do not undergo the phase transition. A void or nonstoichiometric fraction of order a few percent is consistent with the model results; however, confirmation would require THz or percolation measurements of void fractions over a range of thicknesses.

The calculated transmission takes into account the finite thickness of both substrate and thin film, as described in Sec. II B. The strong oscillations seen both in the transmission amplitude and phase shift spectra are due to multiple reflections of the THz wave inside the substrate. At elevated temperatures the high carrier concentration in the thin film enhances the reflectivity of one of the surfaces of the substrate, leading to a higher optical finesse compared to the bare portion of the substrate, which has a relatively constant index of refraction of 3.5 over the THz frequency range and a thickness of 150 μm.

The shape of the calculated spectra allows a comparison of the performance of the two EMT's considered here. The shapes of the measured transmission amplitude spectrum and the phase shift spectrum (Fig. 4), as well as their absolute magnitude, resemble those calculated by Maxwell-Garnett EMT, whereas the agreement between our experiment and predictions by Bruggeman EMT is much less convincing. In particular, the phase predicted by the Bruggeman EMT predicts oscillations about zero as a function of frequency, while that predicted by Maxwell-Garnett remains uniformly positive. According to the Maxwell-Garnett EMT the transmission should decrease and the phase shift should increase with the frequency, whereas the Bruggeman EMT predicts a relatively constant transmission drop and phase shift with frequency.

In Fig. 8 the transmission amplitude and phase shift, averaged over the frequency band 0.3–1.2 THz, is shown as a function of the temperature, using the same parameters as in Fig. 7. The upper panel shows the prediction from Maxwell-Garnett EMT and the lower panel shows the prediction from Bruggeman EMT. The Maxwell-Garnett EMT predicts that the THz transmission amplitude should display a higher transition temperature than the THz phase shift, and that both

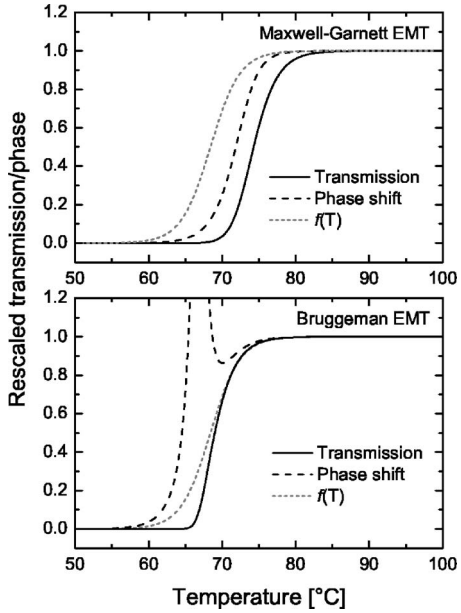

FIG. 8. Average transmission amplitude (solid line) and phase shift (long dashes) in the frequency range 0.3–1.2 THz, calculated with Maxwell-Garnett EMT (upper panel) and Bruggeman EMT (lower panel). The volume fraction $f(T)$ of the conductive domains is shown as a short-dashed curve in each panel.

these transition temperatures should be significantly higher than the structural transition temperature. The Bruggeman theory predicts a different behavior, with a transmission amplitude transition temperature close to the structural one, and a phase behavior displaying a strong, nonmonotonic feature near the percolation point ($f=1/3$ for spherical inclusions), which is below the structural transition temperature at $f=1/2$. Comparison with the experimental data in Fig. 5 directly shows that the different transition temperatures of the transmission amplitude and the phase shift, as well as the elevated switching temperatures in general observed in the THz range, are elegantly explained by Maxwell-Garnett EMT, whereas the Bruggeman EMT fails to reproduce these observations.

The rather poor agreement between Bruggeman EMT and the observed behavior of the dielectric function of the thin VO_2 film in the THz range is at first glance unexpected. Recently Choi *et al.* used Bruggeman EMT to explain mid-infrared spectroscopic investigations of the VO_2 phase transition.[4] In their work the percolation behavior built into the Bruggeman EMT was found to be important for the interpretation of the experimental results. At the percolation point the Bruggeman EMT predicts that a macroscopic conductive path opens up, and this is expected to change the electric properties of the thin film dramatically. In our work we use THz spectroscopy to probe the high-frequency conductivity of the thin film in a contact-free manner, making it possible to determine the dielectric function of isolated domains without electric contact to the surroundings. This appealing property of THz-TDS has earlier been used in the characterization of photoexcited charge carriers in insulators.[20,21] This clearly indicates that the conductivity determined by THz-TDS is independent of the formation of a macroscopic conductive path throughout the sample. Very likely this is the reason why the Bruggeman EMT seems less appropriate for the description of the macroscopic THz dielectric function of VO_2 films although this EMT has been used with success to explain both dc measurements and mid-infrared spectroscopic results.

Very recently, Cooke *et al.* convincingly showed that the Drude-Smith model is applicable for the description of the transient dielectric properties following optical excitation of nanometer-sized silicon nanocrystals.[22] Although there are striking principal similarities between their samples and our samples, we believe that the differences in interpretation can be explained by different sizes of the conductive domains in the samples. The silicon nanoparticles investigated by Cooke *et al.* have dimensions of a few nanometers, while the conductive regions in the vanadium dioxide films investigated here may have significantly larger dimensions because of the 160–nm film thickness. Therefore, confinement effects such as preferred backscattering will play a much more dominant role in the interpretation of their results.

VI. CONCLUSIONS

In this work we have used THz spectroscopy to measure the high-frequency conductivity during the semiconductor-to-metal phase transition in VO_2. The THz range was chosen for this study since frequencies in this range are high enough to offer a contact free, and therefore local, probe of the high-frequency conductivity of the sample, and low enough to be below the phonon modes of the crystal lattice. By measuring both the frequency-dependent transmission amplitude and phase shift we can follow the gradual growth of conductive domains as the temperature is increased towards and above the structural transition temperature. We observe that the onset of changes in the dielectric properties at THz frequencies occur at significantly higher temperatures than in the visible range, and that the transmission amplitude switches at a slightly higher temperature than the phase shift of the transmitted light. Furthermore, the sign of the phase shift through the VO_2 film above the transition temperature is opposite of that expected for a homogeneous, conducting film. All these observations are explained by the application of effective-medium theory, and in particular we find that the Maxwell-Garnett EMT is capable of reproducing all aspects of the experimental data with realistic parameters for the conductive domains. We also find that the simplest Drude model is better suited for the description of the high-frequency conductivity of the metallic domains in VO_2 than the generalized Drude-Smith model that is often used in the description of the low-frequency conductivity of a poor conductor.

The spectroscopic approach used in this work, as well as in previous optical and electrical studies of the phase transition in VO_2, are based on a macroscopic description of the dielectric properties of the material. Techniques for the characterization of dielectric properties on a scale smaller than the domain sizes would offer an extremely interesting view of the dynamics of domain growth associated with phase transitions.

ACKNOWLEDGMENTS

The authors acknowledge fruitful discussions with Mischa

Bonn and David Cooke. The authors also thank Leonard Feldman for helpful discussions about the film characteristics. Research at Vanderbilt was partially supported by the National Science Foundation Grant No. (DMR-0210875) and the Vanderbilt Academic Venture Capital Fund. Research at Freiburg University was supported by a grant from the Ministry of Science, Research and the Arts of Baden-Wrttemberg 24-7532.23-11-11/1. Research at the Technical University of Denmark was partially supported by the EU Integrated Project TeraNova.

---

*Present address: Department of Physics and Astronomy and Institute for Advanced Materials, Nanoscience and Technology, University of North Carolina, Chapel Hill, NC 27599, USA.

[1] F. J. Morin, Phys. Rev. Lett. **3**, 34 (1959).
[2] R. Lopez, T. E. Haynes, L. A. Boatner, L. C. Feldman, and R. F. Haglund, Jr., Phys. Rev. B **65**, 224113 (2002).
[3] P. J. Hood and J. F. DeNatale, J. Appl. Phys. **70**, 376 (1991).
[4] H. S. Choi, J. S. Ahn, J. H. Jung, T. W. Noh, and D. H. Kim, Phys. Rev. B **54**, 4621 (1996).
[5] J. Rozen, R. Lopez, R. F. Haglund, Jr., and L. C. Feldman, Appl. Phys. Lett. **88**, 081902 (2006).
[6] D. A. G. Bruggeman, Ann. Phys. **24**, 636 (1935).
[7] J. C. Maxwell Garnett, Philos. Trans. R. Soc. London **205**, 237 (1906).
[8] J. I. Gittleman and B. Abeles, Phys. Rev. B **15**, 3273 (1977).
[9] E. Hendry, M. Koeberg, B. O'Regan, and M. Bonn, Nano Lett. **6**, 755 (2006).
[10] M. Schall and P. Uhd Jepsen, Opt. Lett. **25**, 13 (2000).
[11] M. Schall, M. Walther, and P. U. Jepsen, Phys. Rev. B **64**, 094301 (2001).
[12] M. Walther, B. Fischer, H. Helm, and P. Uhd Jepsen, Chem. Phys. Lett. **332**, 389 (2000).
[13] M. Born and E. Wolf, *Principles of Optics*, 7th ed. (Cambridge University Press, Cambridge, 1999).
[14] N. V. Smith, Phys. Rev. B **64**, 155106 (2001).
[15] G. M. Turner, M. M. Beard, and C. A. Schmuttenmaer, J. Phys. Chem. B **106**, 11716 (2002).
[16] M. van Exter, Ch. Fattinger, and D. Grischkowsky, Opt. Lett. **14**, 1128 (1989).
[17] R. Lopez, L. C. Feldman, R. F. Haglund, Jr., T. E. Haynes, and L. A. Boatner, Appl. Phys. Lett. **85**, 5191 (2004).
[18] M. Rini, A. Cavelleri, R. W. Schoenlein, R. Lopez, L. C. Feldman, R. F. Haglund, Jr., L. A. Boatner, and T. E. Haynes, Opt. Lett. **30**, 558 (2005).
[19] J. Y. Suh, R. Lopez, L. C. Feldman, and R. F. Haglund, Jr., J. Appl. Phys. **96**, 1209 (2004).
[20] E. Knoesel, M. Bonn, J. Shan, and T. F. Heinz, Phys. Rev. Lett. **86**, 340 (2001).
[21] J. Shan, F. Wang, E. Knoesel, M. Bonn, and T. F. Heinz, Phys. Rev. Lett. **90**, 247401 (2003).
[22] D. G. Cooke, A. N. MacDonald, A. Hryciw, J. Wang, Q. Li, A. Meldrum, and F. A. Hegmann, Phys. Rev. B **73**, 193311 (2006).